This manuscript was accepted by Appl. Phys. Lett. Click here to see the version of record.

Two-Dimensional MoS_2 Negative Capacitor Transistors for Enhanced (Super-Nernstian) Signal-to-Noise Performance of Next-generation Nano Biosensors

N. Zagni,[1,2] P. Pavan,[2] and M. A. Alam[1,a)]
[1)] *School of Electrical and Computer Engineering, Purdue University, West Lafayette, Indiana 47907, USA*
[2)] *Department of Engineering "Enzo Ferrari", University of Modena and Reggio Emilia, Modena, 41125, Italy*

The detection of biomolecules by a Field Effect Transistor-based biosensor (BioFET) is dictated by the sensor's intrinsic Signal-to-Noise Ratio (*SNR*). The detection limit of a traditional BioFET is fundamentally limited by biomolecule diffusion, charge screening, linear charge to surface-potential transduction, and Flicker noise. In this letter, we show that the recently introduced class of transistors called Negative Capacitor Field effect transistor (NCFET) offers nonlinear charge transduction and suppression of Flicker noise to dramatically improve the *SNR* over classical Boltzmann sensors. We quantify the *SNR* improvement (approximately two orders of magnitude higher than a classical Si-NW biosensor) by interpreting the experimental results associated with the signal and noise characteristics of 2D MoS_2-based transistors. The proposed NC-BioFET will motivate experimentalists to combine two well-established technologies to achieve high *SNR* (and to improve the detection limit), fundamentally unachievable by any other sensor technology.

Over the last 50 years, many groups worldwide have dedicated their research to develop highly sensitive, fast responding, and selective transistor-based biosensors. These sensors, known as BioFETs, allow label-free detection of biomolecules with the Limit of Detection (LOD) in the nano- and pico- molar concentration ranges[1], potentially enabling many applications in personalized medicine[2], early detection of diseases[3], genome sequencing[4,5], etc. A BioFET relies on the modulation of surface potential due to the charged biomolecules adsorbed on the gate electrode. Thus, the fundamental sensitivity limit of BioFETs depends on the diffusion of biomolecules[6], surface charge screening, and linear "charge-to-surface potential" relationship[7]. These limitations apply to all FET-based biosensors, e.g., Dual-Gate FET[8]; Silicon Nanowire (Si-NW)[1,7,9]; coupled Nanoplate-Nanowire (NW-NP)[10]; 2D-semiconductors FET[11–13]. In contrast, electro-mechanically actuated biosensors obviate the screening effect and enhance the sensitivity and Signal-to-Noise Ratio (*SNR*)[14] through their inherent nonlinear "mass-vs-deflection" response[15–17]. Unfortunately, the sensitivity improvement is counterbalanced by the difficulty of integrating these sensors into low-voltage CMOS integrated circuits[18,19]. Moreover, sensors based on dynamic mechanical response must be driven by complex oscillator circuits, further exacerbating the integration challenge.

In this letter, we show that the recently proposed negative-capacitor field-effect transistor (NCFET) could enhance sensitivity beyond the Nernst limit, making this CMOS-compatible device an attractive alternative to the nonlinear electro-mechanical biosensors. The NCFET was originally proposed to reduce the sub-threshold slope (and the power dissipation) of the Metal-oxide field-effect transistors (MOSFETs)[20,21]; however, the inherent non-linearity of NCFETs – arising from the nonlinear negative derivative of polarization vs. field characteristics of a ferroelectric capacitor – can also be exploited to enhance the sensitivity of biosensors. Most importantly, NCFETs can improve the *SNR* compared to traditional MOSFETs by suppressing the low frequency flicker noise related to carrier number fluctuations[22]. Finally, since NCFETs are fabricated by a simple process-modification that converts standard HfO_2 into a ferroelectric film[23,24], they should be easily integrated into the standard CMOS process flow for realizing nanoscale biosensors.

We thus introduce the concept of the NC-BioFET, combining the NCFET with the conventional BioFET to obtain improved sensitivity and enhanced *SNR*. To this end, we develop an analytical model of the NC-BioFET to predict the performance of this class of sensors. Our results show that despite the fundamental limits of charged-based BioFETs[8,10], the NC-BioFET could dramatically improve the label-free detection of biomolecules. Our analysis, based on nontrivial integration of two well established technologies (i.e., NCFET and BioFET), provides the theoretical foundation necessary for the experimental demonstration of the NC-BioFET. Although we focus on nanobiosensing, the principle of negative capacitance based detection is general and can improve, for example, the *SNR* of potentiometric transistor-based gas sensors[25].

The physical model developed in this work focuses on three fundamental mechanisms: (*i*) the screening of the electrolyte solution (representing the 'sensing' part of the device); (*ii*) the nonlinear response of the negative capacitor and; (*iii*) electrical response of the transistor. This modeling approach integrates the negative capacitor with the conventional MOSFET and with the electrolyte model, thereby simplifying the design of NC-BioFETs. The model is discussed in detail in the supplementary material. We illustrate the principle of operation of the NC-BioFET by using a Molybdenum Disulfide (MoS_2) field-effect transistor. The choice of this particular class of transistors is motivated by: (*i*) the experimental demonstration of NCFETs realized in this technology[22,26,27]; and (*ii*) the investigation of possible biosensing applications for MoS_2 FETs[11–13], because of their potential for integration

a)Corresponding Author: alam@purdue.edu

in ultra-scaled devices and excellent electrostatic control[12,22]. Fig. 1(a) shows the BioFET configuration involving a MoS_2 FET, with the negative capacitor layer included in the gate stack of the MOSFET. The MoS_2 FET may be exposed to the fluidic environment either indirectly via the gate oxide layer[12,13], or directly through the channel[11]. In this work, we consider the ferroelectric as the layer exposed to the fluidic environment. The metal gate is replaced by the electrolyte and by the reference electrode as in common BioFET configurations. The electrolyte is modeled based on the derivation in ref.[28] for a pH sensor. The effect of charged biomolecules, Q_{BIO}, is included in the charge neutrality equation as follows:

$$Q_{dl} + Q_{surface} + Q_{BIO} + Q_{MOS} = 0 \tag{1}$$

where Q_{dl} is the double-layer charge, $Q_{surface}$ is the surface charge due to screening effects and Q_{MOS} is the MOSFET charge. In a first-order approximation Q_{MOS} can be neglected as $Q_{surface}$ almost entirely neutralizes Q_{dl} and Q_{BIO}[28]. This phenomenon is at the origin of the so-called screening limited response of FET-based biosensors[7]. Site-binding model parameters[29] are taken by considering HfO_2 as the interfacial insulator with the electrolyte. The model takes also into account the screening due to salt ions in the solution and the additional potential drop due to the finite size of charges building up at the interface with the oxide (i.e., the so-called Stern layer)[28,30] .

To model the non-linear negative capacitor, we use the well-known phenomenological Landau-Khalatnikov (LK) equation[20,31]:

$$V_{NC}/t_{NC} = 2\alpha Q_{MOS} + 4\beta Q_{MOS}^3 + 6\gamma Q_{MOS}^5 + \rho \frac{dQ_{MOS}}{dt} \tag{2}$$

where t_{NC} is the negative capacitor thickness and, α, β, γ, ρ are material and process specific parameters[32,33]. The ferroelectric material under consideration is Zr- doped HfO_2 (i.e., HZO). The parameter values used for the simulations are summarized in the supplementary material. For the DC sensitivity gain of a NCFET compared to a classical biosensor, we need not consider the last term in Eq. (2). This term, however, is important for the AC/noise analysis to account for the ferroelectric contribution to the overall power spectral density, as explained later in the discussion. The gate electrostatics of the NCFET is modeled by following the approach in ref.[32]. This approach considers the negative capacitor and the underlying MOSFET as independent entities connected by a metal interlayer and coupled by the self-consistent solution of the gate electrostatics. Although the metal interlayer is often omitted during process integration[34], it is considered here to simplify the analysis. However, its omission is unlikely to affect the key conclusions as explained as follows. First, the low V_{DS} used commonly for biosensors (to ensure operation in the linear regime) alleviates the potential issue of non-uniform channel potential when the metal interlayer is not present[35]. Second, the gate leakage - which can lead to depolarization fields in the presence of the metal interlayer - is presumed negligible for sufficiently thick gate oxide, as was shown to be case for recently demonstrated 2D NCFETs[26,32].

The negative capacitor provides a voltage amplification between the internal MOSFET potential V_{MOS} and the applied gate voltage V_G. This voltage gain is defined as:

$$A_V \equiv \frac{dV_{MOS}}{dV_G} = \frac{|C_{NC}|}{|C_{NC}| - C_{MOS}} \tag{3}$$

with the symbols of the schematic circuit defined in Fig. 1(b). The C_{NC} expression can be obtained from Eq. (2) by differentiating with respect to Q_{MOS}, $C_{NC}^{-1} = t_{NC}(2\alpha + 12\beta Q_{MOS}^2 + 30\gamma Q_{MOS}^4)$. Note that the gate-voltage dependence of the "effective" permittivity of the ferroelectric is accounted for by the higher-order Landau coefficients β and γ.

The increased sensitivity reflects the cancellation of the ferroelectric negative capacitance by the equivalent MOSFET positive capacitance, i.e., $|C_{NC}| = C_{MOS}$[31]. In this condition, the voltage gain A_V exhibits a strong peak, see Fig. 1(b). The peak occurs only if the negative capacitor layer (t_{NC}) is sufficiently thick to compensate the traditional dielectric, as seen in the $I_D - V_{FG}$ characteristics, Fig. 1(c). The dielectric and ferroelectric thicknesses must be tailored carefully to control the degree of hysteresis present in the $I_D - V_{FG}$ characteristics[20,26] and the corresponding gain in the NC-BioFET sensitivity. An approximate closed-form expression for V_{FG} at the critical point can be written as follows[36]:

$$\begin{aligned} V_{G,CP} =& V_{FB0} + \frac{k_B T}{q} \ln\left(-\frac{k_B T}{q}\frac{1}{(2\alpha t_{NC} + 1/C_{ox})}\frac{1}{qN_{2D}}\right) + \\ & - \frac{k_B T}{q} - \frac{qN_d}{C_{ox}} \\ V_{FG,CP} =& \psi_e + V_{G,CP} \end{aligned} \tag{4}$$

where V_{FB0} is the flat-band voltage, q is the elementary charge, k_B is the Boltzmann constant, T is the temperature, N_{2D} is the 2D semiconductor density of states and ψ_e is the potential drop given by the electrolytic solution[28] (the derivation is given in the supplementary material).

In order to probe the instability region, measurements should be taken by sweeping the front-gate voltage, V_{FG}, (i.e., the potential applied to the floating electrode) for different biomolecule concentrations. With increasing t_{NC}, the drain current switches abruptly from the off- to the on- state as a consequence of improved capacitance matching. For the parameters considered in this work, a 75 nm thick negative capacitance layer is needed for significant potential amplification and enhanced sensitivity. As an aside, we realize that the thickness-dependent polarization of HZO depends on the deposition technique[37,38]. Therefore, in general the design of NC-BioFET should focus on seeking the matching condition $|C_{NC}| = C_{MOS}$, regardless of the particular ferroelectric thickness required to achieve it.

The instability at the critical point leads to the increase in sensitivity, as shown in Fig. 2(a). Sensitivity is defined as the ratio between the current before and after the capture of biomolecules, i.e.: $S = I_{before}/I_{after}$. Here, we consider negatively charged biomolecules (e.g., DNA) that increase the threshold voltage and shift the I-V characteristics to the right.

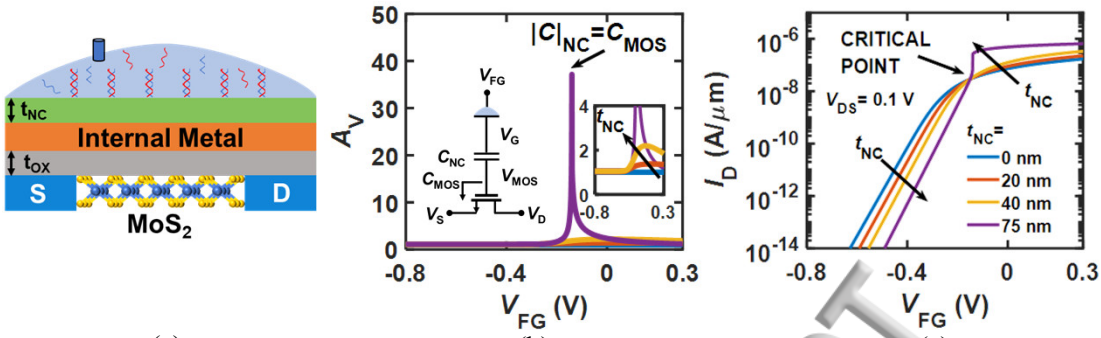

(a) (b) (c)

FIG. 1. (a) Cross-section schematic representation of the NC-BioFET under study. Note that the electrolytic solution lies on the ferroelectric layer. (b) Voltage gain A_V vs. V_{FG} shows a peak when the matching condition is satisfied, i.e., $|C_{NC}| = C_{MOS}$ (symbols are explained in the circuit schematic, see also Eq. (3) in the main text). The inset shows the increase in A_V with increasing t_{NC}. (c) $I_D - V_{FG}$ characteristics for different t_{NC} showing the abrupt transition at the critical point when the t_{NC} is thick enough. All the I-V curves on the paper are taken at V_{DS}0.1 V. The device with $t_{NC} = 0$nm is equivalent to a conventional BioFET and serves as a reference for NC-BioFET.

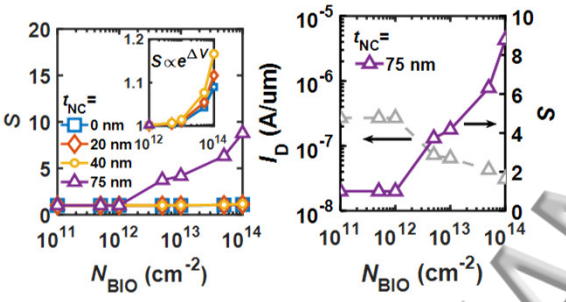

(a) (b)

FIG. 2. (a) Sensitivity vs. biomolecule concentration N_{BIO} with different t_{NC}. The sensitivity suddenly increases due to the current transition from inversion to sub-threshold region for the $t_{NC} = 75$nm case. This transition is shown clearly in (b). The inset in (a) shows a magnification of the plot, indicating that if t_{NC} is not thick enough the sensitivity follows an exponential dependence on the potential shift caused by biomolecules, as one expects in the sub-threshold regime.

The shift in the drain-current due to increasing concentration of captured biomolecules (N_{BIO}) triggers the abrupt transition from inversion to sub-threshold operation, thereby producing a significant change in drain current, see Fig. 2(b). The plots in Fig. 2 are taken at the critical point condition, highlighting the fact that the steep sensitivity increase is obtained when the capacitances are matched (i.e. $t_{NC} = 75$nm). Note that one must scan I_D by sweeping V_{FG} to achieve the improved gain promised by the NC-BioFET. As expected, the response of the NC-BioFET is indistinguishable from a conventional BioFET as long as the instability is absent (i.e., for low N_{BIO}), see the inset in Fig. 2(a). This can be understood by the fact that the screening is still the limiting factor for the response to the capture of biomolecules[10].

We now discuss the reduction in noise of the NC-BioFETs. To evaluate the overall noise of the system, we consider the noise sources separately and obtain the output power spectral density by summing up the single contributions (assuming statistical independence between the individual processes). To avoid confusion with the symbol for sensitivity S, we refer to the noise power spectral density with *PSD*. The electrolytic solution contributes with thermal noise due its finite conductivity[28]. The negative capacitor contributes to the overall *PSD* with thermal noise associated with dissipative process due to the damped ferroelectric switching[39], and can be quantified from the last term in Eq. (2). The transistor contributes both thermal and flicker ($1/f$) noise[40]. The thermal noise of the MOSFET is caused by the carriers flowing in a resistive-like channel, whereas Flicker noise arises due to the fluctuation of the number and mobility of carriers in the channel due to the occurring of trapping/detrapping events at the interface with the gate oxide. The general model for the flicker noise in MOSFETs[41] must be modified to obtain an expression that takes into account the negative capacitance effect, i.e.:

$$PSD_{I_D,1/f} = \frac{q^2 \lambda k_B T N_t}{f W L C_{eq}^2} \left(1 + \alpha_C \mu_{eff} C_{ox} \frac{I_D}{g_m}\right)^2 g_m^2 \qquad (5)$$

where f is the frequency, λ is the tunneling length, N_t is the oxide traps density, C_{eq} ($C_{eq}^{-1} = C_{NC}^{-1} + C_{ox}^{-1}$) is the equivalent oxide capacitance, g_m is the transconductance, μ_{eff} is the carriers' effective mobility, and α_C is the Coulomb scattering coefficient.

Fig. 3(a) shows that Eq. (5) qualitatively anticipates the counter-intuitive thickness-dependent suppression of the noise spectra observed in the experiments[22], demonstrating the beneficial effect of the ferroelectric layer in terms of noise reduction. The noise contributions due to the electrolyte, ferroelectric and MOSFET channel are found to be negligible compared to the Flicker noise of the transistor, hence they are not a limiting factor for the *SNR*. More details regarding the interpretation of the Flicker Noise reduction and the noise sources are found in the supplementary material.

The total drain current *PSD* (normalized to the square of the DC current) is shown in Fig. 3(b), with a clear decreasing trend with increasing t_{NC}. The reason for the *PSD* reduction with increasing t_{NC} is related to the reduction of the Flicker

This manuscript was accepted by Appl. Phys. Lett. Click here to see the version of record.

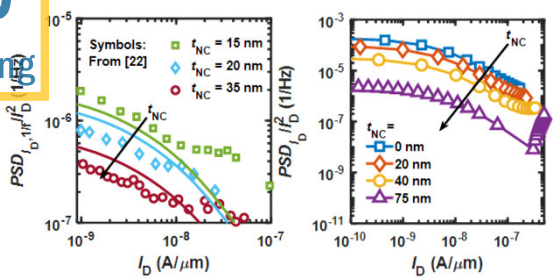

FIG. 3. (a) Comparison of model from Eq. (5) with experimental data[22] by using $C_{eq} = C_{ox} \parallel C_{NC}$, showing the decreasing trend with increasing t_{NC}. (b) Total normalized drain current *PSD* showing clear reduction with increasing t_{NC} due to the Flicker noise (i.e., the dominant noise source) reduction.

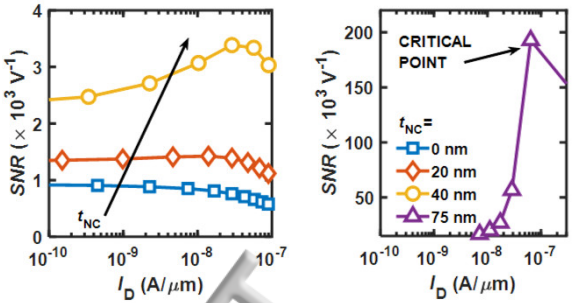

FIG. 4. Intrinsic *SNR* trend with increasing t_{NC} for (a) small negative capacitor thickness and (b) high t_{NC} (that triggers the abrupt switching of the current at the critical point). The *SNR* shows qualitatively an opposite behavior to the normalized *PSD* (even for small t_{NC}) which can be attributed to the Flicker noise reduction. Note that for $t_{NC} = 75$ nm, the *SNR* peaks at the peak of g_m.

noise, as discussed previously. The increased equivalent oxide capacitance at the denominator in Eq. (5) explains the reduction in the noise, and it is in agreement with experimental observations [see Fig. 3(a)]. The noise reduction provided by the negative capacitor is particularly important for biosensors given the difficulty in providing low noise amplifiers on small geometries due to the high value of the intrinsic flicker noise[42].

The Flicker noise reduction, along with the sensitivity increase, leads to the improved SNR defined as following[43]:

$$SNR = \frac{\Delta I_D}{\delta I_{D,n}} \tag{6}$$

where ΔI_D is the difference between the current before and after the capture of biomolecules, and $\delta I_{D,n}$ is the noise signal superimposed to the DC value, calculated from the total noise *PSD* as $\delta I_{D,n} = \sqrt{\int PSD_{I_D} df}$. Note that the *SNR* can be more conveniently expressed per unit voltage (considering that $\Delta I_D \sim g_m \Delta V_{FG}$ and normalizing by ΔV_{FG}) to have a quantitative expression for the intrinsic *SNR*, independent of the input signal.

Fig. 4(a) shows that the increase in t_{NC} improves the intrinsic *SNR* for all regions of operation. For $t_{NC} = 75$ nm, the NC-BioFET reaches a maximum *SNR* of $\sim 2 \times 10^5$ V^{-1} that is almost two orders of magnitude higher than that of a Silicon Nanowire BioFET[43] [see Fig. 4(b)]. Although this remarkably high sensitivity (and thus *SNR*) is achieved with a relatively thick ferroelectric (i.e. 75 nm), typical long channel biosensors can easily accommodate such a thick film[12,28]. It is also possible to reduce the ferroelectric thickness in NC-BioFETs and still obtain the same benefits in terms of *SNR* by properly doping the HfO_2 layer. For example, as shown in the supplementary material, by using Si instead of Zr as the doping atoms for HfO_2 one can use a ferroelectric with $t_{NC} = 16$ nm and still obtaining similar *SNR* peak compared to the case with HZO. This result shows that the NC-BioFETs can be scaled to realize nano-biosensors with enhanced *SNR*.

We mention the fact that the performance improvement of the NC-BioFET is affected by the interface traps and quantum gate capacitance. In general, the effect of interface traps and of quantum capacitance is to increase the sub-threshold slope and to lower the total gate capacitance, respectively. Thus, the sensitivity of the NC-BioFET can reduce because of the deteriorated capacitance matching between the ferroelectric and underlying MOS, which lowers the voltage gain as defined in Eq. (3). Hence, to avoid performance degradation of the NC-BioFET, design strategies (such as employing a thicker ferroelectric) would be required to compensate for the reduction in capacitance matching.

To summarize, we have proposed the concept of NC-BioFETs as a class of biosensors that exploits the negative capacitance (phase transition) effect to improve the Signal-to-Noise Ratio (*SNR*). As the baseline device, we considered the 2D semiconductor FET given its applicability for next-generation ultra-scaled biosensors. We found that, upon the triggering of the non-linear effects associated with the negative capacitance, the sensitivity of NC-BioFETs is significantly improved compared to a traditional nanobiosensor. At the same time, Flicker noise of the transistor is reduced as a result of the increase in the equivalent gate oxide capacitance, thereby improving the *SNR*. Finally, by properly choosing the dopant atoms for the ferroelectric HfO_2, it is possible to reduce the ferroelectric thickness while still obtaining the instability required to improve *SNR*, thereby enabling the scalability of NC-BioFETs with current CMOS processes.

SUPPLEMENTARY MATERIAL

See supplementary material for: (*i*) the calibration curves of the 2D FET characteristics with experimental data; (*ii*) details regarding the modeling approach and derivations; and (*iii*) simulation results with the HSiO ferroelectric oxide.

ACKNOWLEDGMENTS

The authors wish to thank Kamal Karda and Prof. Peide Ye (Purdue University) for fruitful discussion.

[1] Y. Cui, Q. Wei, H. Park, and C. M. Lieber, Science Translational Medicine **293**, 1289 (2001).
[2] B. R. Dorvel, B. Reddy, J. Go, C. Duarte Guevara, E. Salm, M. A. Alam, and R. Bashir, ACS Nano **6**, 6150 (2012).
[3] P. Namdari, H. Daraee, and A. Eatemadi, Nanoscale Research Letters **11** (2016), 10.1186/s11671-016-1618-z.
[4] D. A. Wheeler, M. Srinivasan, M. Egholm, Y. Shen, L. Chen, A. McGuire, W. He, Y.-J. Chen, V. Makhijani, G. T. Roth, X. Gomes, K. Tartaro, F. Niazi, C. L. Turcotte, G. P. Irzyk, J. R. Lupski, C. Chinault, X.-z. Song, Y. Liu, Y. Yuan, L. Nazareth, X. Qin, D. M. Muzny, M. Margulies, G. M. Weinstock, R. A. Gibbs, and J. M. Rothberg, Nature **452**, 872 EP (2008).
[5] J. Go and M. A. Alam, Journal of Applied Physics **114**, 164311 (2013).
[6] P. R. Nair and M. A. Alam, Applied Physics Letters **88**, 233120 (2006).
[7] P. R. Nair and M. A. Alam, Nano Letters **8**, 1281 (2008), arXiv:0712.0198.
[8] J. Go, P. R. Nair, and M. A. Alam, Journal of Applied Physics **112** (2012), 10.1063/1.4737604.
[9] J. I. Hahm and C. M. Lieber, Nano Letters **4**, 51 (2004).
[10] J. Go, P. R. Nair, B. Reddy, B. Dorvel, R. Bashir, and M. A. Alam, ACS Nano **6**, 5972 (2012).
[11] J. Lee, P. Dak, Y. Lee, H. Park, W. Choi, M. A. Alam, and S. Kim, Scientific Reports **4**, 7352 (2015).
[12] D. Sarkar, W. Liu, X. Xie, A. C. Anselmo, S. Mitragotri, and K. Banerjee, ACS Nano **8**, 3992 (2014).
[13] H. Nam, B. R. Oh, P. Chen, M. Chen, S. Wi, W. Wan, K. Kurabayashi, and X. Liang, Scientific Reports **5**, 10546 (2015).
[14] A. Jain and M. A. Alam, Applied Physics Letters **105**, 084106 (2014).
[15] A. Jain and M. A. Alam, arXiv preprint arXiv:1305.5729 , 1 (2013).
[16] V. Kumar, J. W. Boley, Y. Yang, H. Ekowaluyo, J. K. Miller, G. T. Chiu, and J. F. Rhoads, Applied Physics Letters **98**, 2009 (2011).
[17] A. Jain, P. R. Nair, and M. A. Alam, Proceedings of the National Academy of Sciences **109**, 9304 (2012).
[18] M. H. Hasan, F. M. Alsaleem, N. Jaber, M. A. Hafiz, and M. I. Younis, AIP Advances **8** (2018), 10.1063/1.5018321.
[19] N. Bajaj, G. T. Chiu, and J. F. Rhoads, Journal of Sound and Vibration **425**, 257 (2018).
[20] S. Salahuddin and S. Datta, Nano Letters **8**, 405 (2008), arXiv:0707.2073.
[21] K. Karda, A. Jain, C. Mouli, and M. A. Alam, Applied Physics Letters **106** (2015), 10.1063/1.4918649.
[22] S. Alghamdi, M. Si, L. Yang, and P. D. Ye, in *IEEE International Reliability Physics Symposium Proceedings* (2018) pp. 3–7.
[23] J. Müller, T. S. Böscke, U. Schröder, S. Mueller, D. Bräuhaus, U. Böttger, L. Frey, and T. Mikolajick, Nano Letters **12**, 4318 (2012).
[24] T. S. Böescke, J. Müller, D. Bräuhaus, U. Schröder, and U. Böttger, Technical Digest - International Electron Devices Meeting, IEDM , 547 (2011).
[25] T. Yoshizumi and Y. Miyahara, in *Different Types of Field-Effect Transistors - Theory and Applications* (InTech, Rijeka, 2017) Chap. 8, pp. 149–163.
[26] M. Si, C. J. Su, C. Jiang, N. J. Conrad, H. Zhou, K. D. Maize, G. Qiu, C. T. Wu, A. Shakouri, M. A. Alam, and P. D. Ye, Nature Nanotechnology **13**, 24 (2018), arXiv:1704.06865.
[27] F. A. Mcguire, Y.-C. C. Lin, K. Price, G. B. Rayner, S. Khandelwal, S. Salahuddin, and A. D. Franklin, Nano Letters **17**, 4801 (2017).
[28] P. Dak, W. Seo, B. Jung, and M. A. Alam, IEEE Transactions on Electron Devices **64**, 1277 (2017).
[29] Ajay, R. Narang, M. Saxena, and M. Gupta, IEEE Transactions on Electron Devices **64**, 1742 (2017).
[30] R. E. G. Van Hal, J. C. T. Eijkel, and P. Bergveld, Advances in Colloid and Interface Science **69**, 31 (1996).
[31] G. Pahwa, T. Dutta, A. Agarwal, S. Khandelwal, S. Salahuddin, C. Hu, and Y. S. Chauhan, IEEE Transactions on Electron Devices **63**, 4986 (2016).
[32] C. Jiang, M. Si, R. Liang, J. Xu, P. D. Ye, and M. A. Alam, IEEE Journal of the Electron Devices Society **6**, 189 (2018).
[33] K. Chatterjee, A. J. Rosner, and S. Salahuddin, IEEE Electron Device Letters **38**, 1328 (2017).
[34] E. Ko, J. Shin, and C. Shin, Nano Convergence **5** (2018), 10.1186/s40580-018-0135-4.
[35] J. P. Duarte, S. Khandelwal, A. I. Khan, A. Sachid, Y. K. Lin, H. L. Chang, S. Salahuddin, and C. Hu, Technical Digest - International Electron Devices Meeting, IEDM **5**, 30.5.1 (2017).
[36] H. P. Chen, V. C. Lee, A. Ohoka, J. Xiang, and Y. Taur, IEEE Transactions on Electron Devices **58**, 2401 (2011).
[37] M. H. Park, H. Joon Kim, Y. Jin Kim, W. Lee, T. Moon, and C. Seong Hwang, Applied Physics Letters **102**, 0 (2013).
[38] M. H. Park, Y. H. Lee, H. J. Kim, Y. J. Kim, T. Moon, K. D. Kim, J. Müller, A. Kersch, U. Schroeder, T. Mikolajick, and C. S. Hwang, Advanced Materials **27**, 1811 (2015).
[39] A. I. Khan, K. Chatterjee, B. Wang, S. Drapcho, L. You, C. Serrao, S. R. Bakaul, R. Ramesh, and S. Salahuddin, Nature Materials **14**, 182 (2015), arXiv:1409.3273.
[40] M. J. Deen, M. W. Shinwari, J. C. Ranuárez, and D. Landheer, Journal of Applied Physics **100** (2006), 10.1063/1.2355542.
[41] M. Von Haartman and M. Östling, in *Low-Frequency Noise in Advanced MOS Devices*, 53 (Springer Netherlands, Amsterdam, 2007) pp. 53–102.
[42] T. C. Nguyen, W. Qiu, M. Altissimo, P. G. Spizzirri, L. H. W. van Beveren, and E. Skafidas, in *Graphene, Carbon Nanotubes, and Nanostructures: Techniques and Applications*, edited by J. E. Morris and K. Iniewski (CRC Press, Boca Raton (FL), 2013) pp. 265 – 278, arXiv:1302.5460.
[43] N. K. Rajan, D. A. Routenberg, and M. A. Reed, Applied Physics Letters **98**, 264107 (2011).

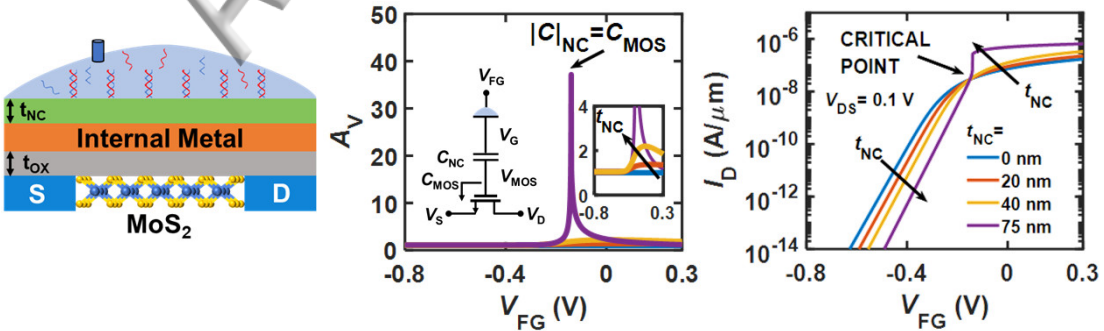
t_NC
Internal Metal
t_OX
S
D
MoS2
|C|NC=CMOS
AV
VFG
VG
CNC
CMOS
VMOS
VS
VD
tNC
VFG (V)
CRITICAL POINT
VDS= 0.1 V
ID (A/μm)
tNC=
0 nm
20 nm
40 nm
75 nm

(a) (b) (c)

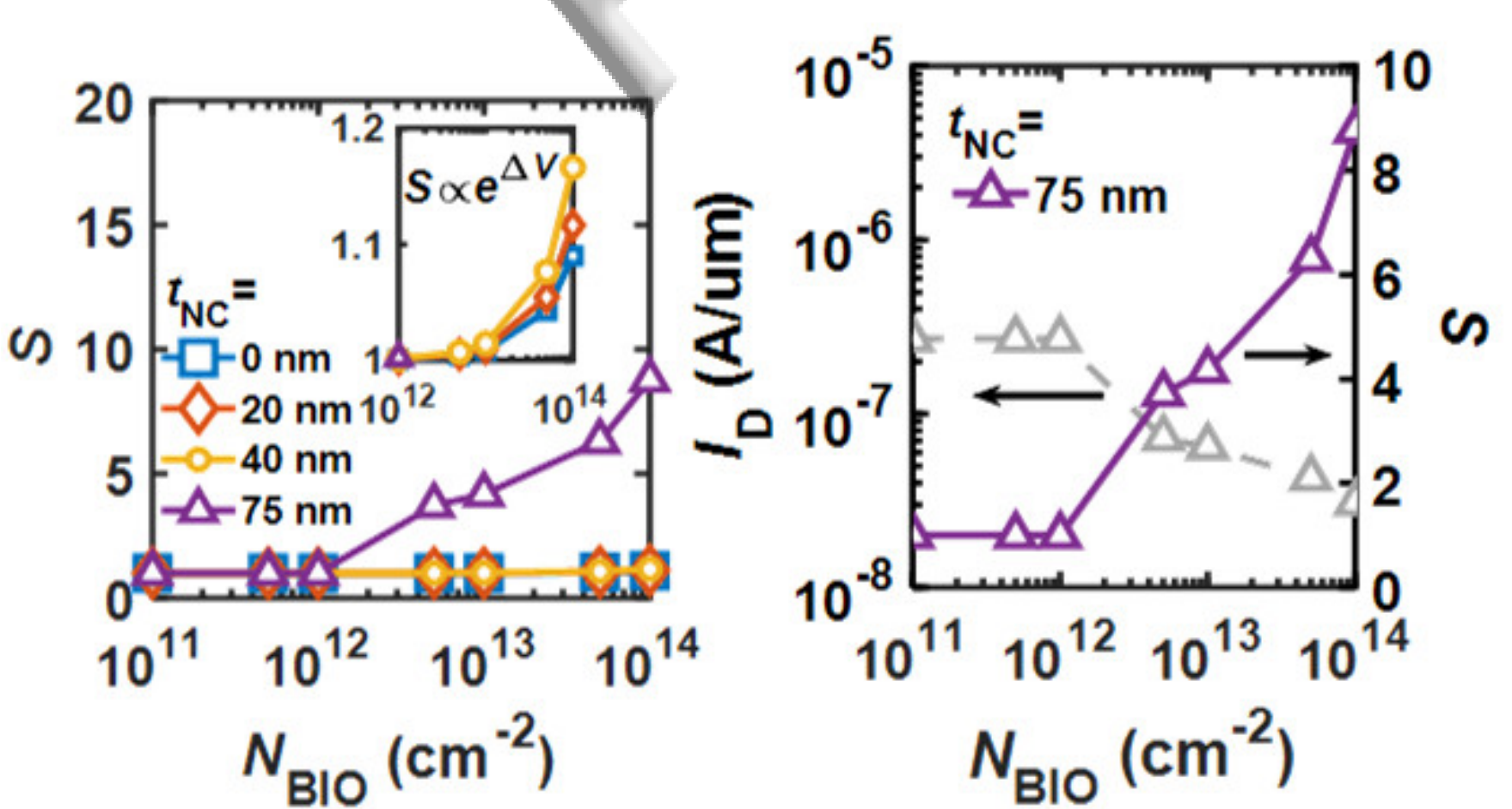
S
20
15
10
5
0
t_{NC}=
0 nm
20 nm
40 nm
75 nm
1.2
1.1
1
$S \propto e^{\Delta V}$
10^{12}
10^{14}
10^{11}
10^{12}
10^{13}
10^{14}
N_{BIO} (cm^{-2})
I_D (A/um)
10^{-5}
10^{-6}
10^{-7}
10^{-8}
t_{NC}=
75 nm
10
8
6
4
2
0
S
10^{11}
10^{12}
10^{13}
10^{14}
N_{BIO} (cm^{-2})

(a) (b)

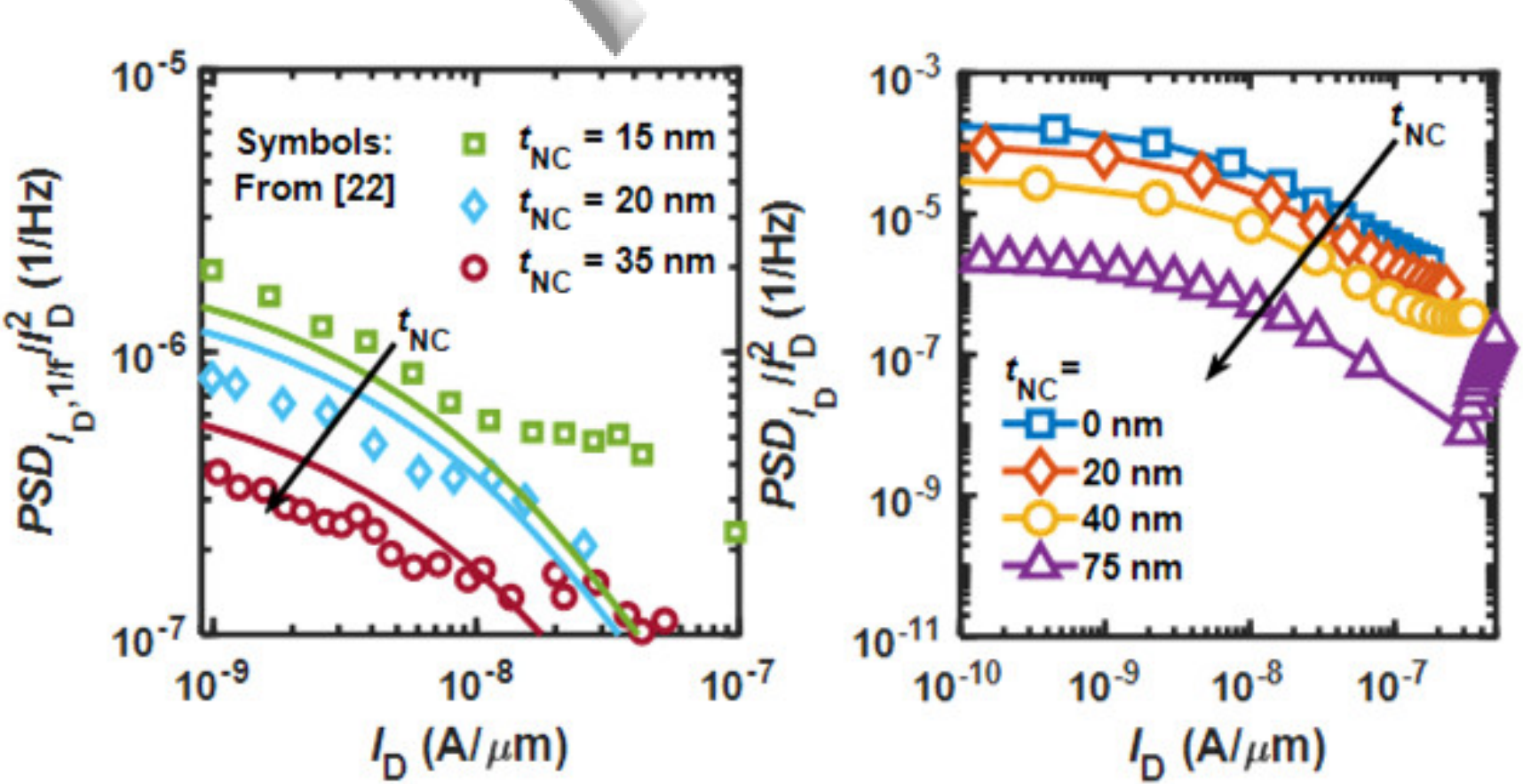
Symbols:
From [22]
t_{NC} = 15 nm
t_{NC} = 20 nm
t_{NC} = 35 nm
t_{NC}
$PSD_{I_D,1/f}/I_D^2$ (1/Hz)
I_D (A/μm)
t_{NC}
t_{NC} =
0 nm
20 nm
40 nm
75 nm
PSD_{I_D}/I_D^2 (1/Hz)
I_D (A/μm)

(a) (b)

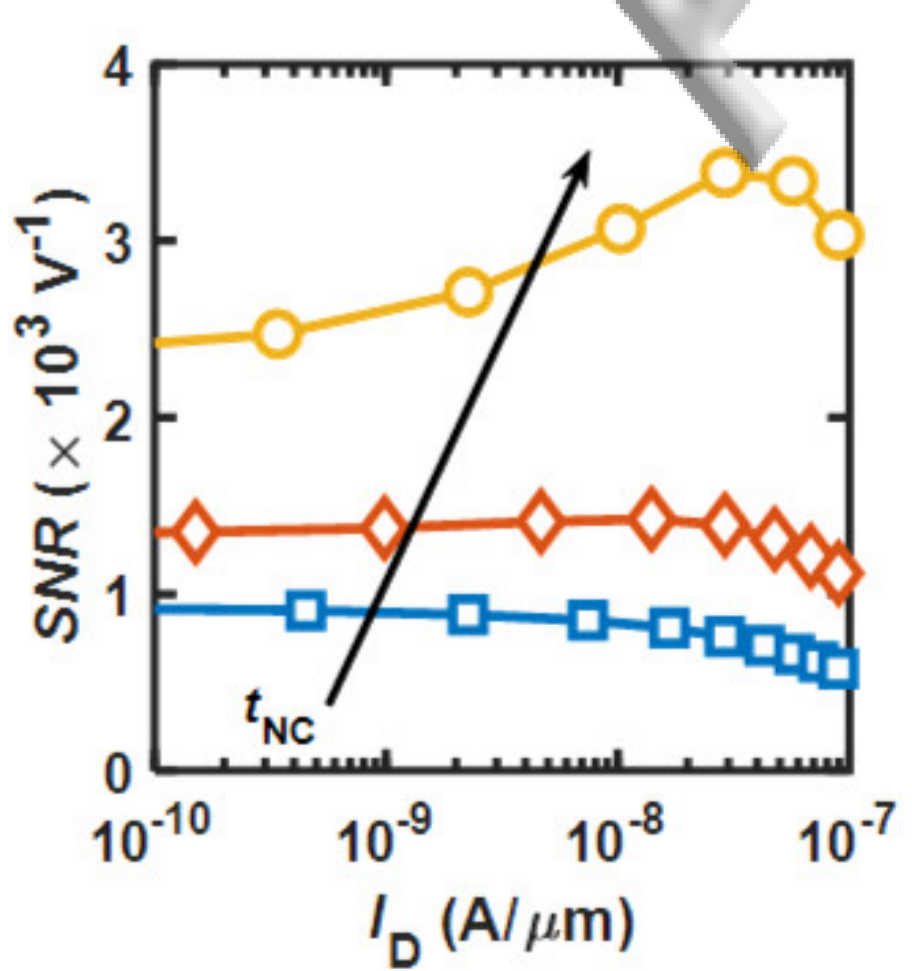
4
3
2
1
0
SNR (× 10^3 V^-1)
t_NC
10^-10
10^-9
10^-8
10^-7
I_D (A/μm)

(a)

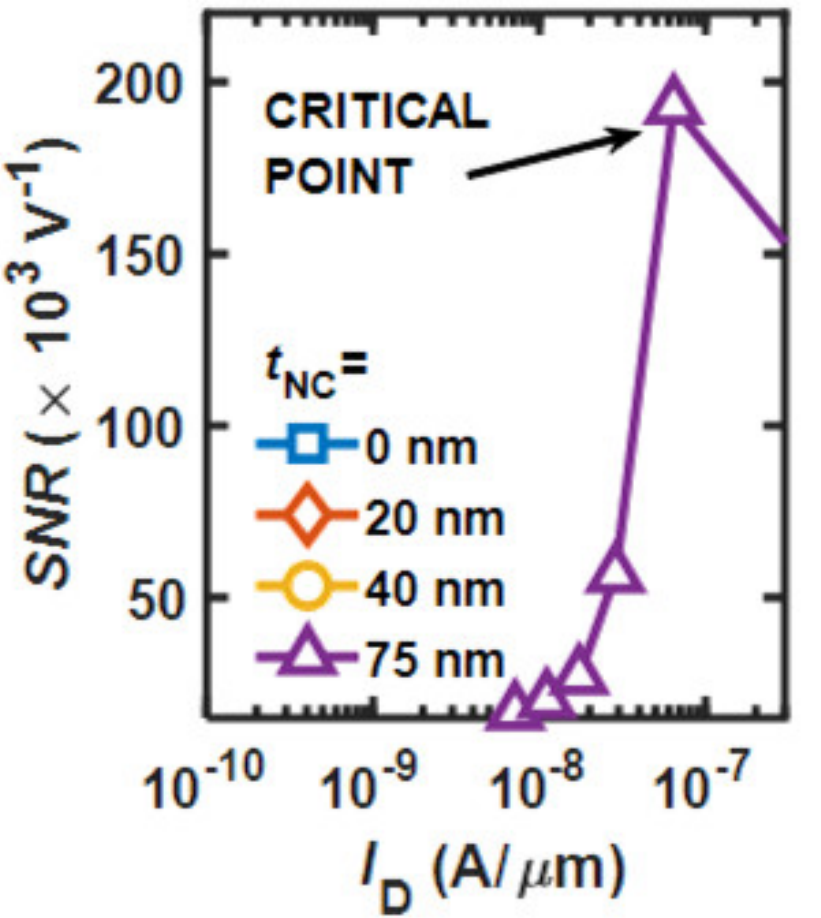
200
150
100
50
SNR (× 10^3 V^-1)
CRITICAL
POINT
t_NC=
0 nm
20 nm
40 nm
75 nm
10^-10
10^-9
10^-8
10^-7
I_D (A/μm)

(b)